Received: 26 April 2020 | Revised: 5 August 2020 | Accepted: 5 August 2020

DOI: 10.1111/joa.13302

ORIGINAL PAPER

ANATOMICAL SOCIETY Journal of Anatomy WILEY

The claustrum of the sheep and its connections to the visual cortex

Andrea Pirone[1] | Jean-Marie Graïc[2] | Enrico Grisan[3,4] | Bruno Cozzi[2]

[1]Department of Veterinary Sciences, University of Pisa, Pisa, Italy

[2]Department of Comparative Biomedicine and Food Science, University of Padova, Legnaro, Italy

[3]Department of Information Engineering, University of Padova, Vicenza, Italy

[4]School of Engineering, London South Bank University, London, UK

Correspondence
Jean-Marie Graïc, Department of Comparative Biomedicine and Food Science, University of Padova, viale dell'Università 16, 35020 Legnaro, PD, Italy.
Email: jeanmarie.graic@unipd.it

Funding information
Università degli Studi di Padova, Grant/Award Number: 2015Y5W9YP

Abstract

The present study analyses the organization and selected neurochemical features of the claustrum and visual cortex of the sheep, based on the patterns of calcium-binding proteins expression. Connections of the claustrum with the visual cortex have been studied by tractography. Parvalbumin-immunoreactive (PV-ir) and Calbindin-immunoreactive (CB-ir) cell bodies increased along the rostro-caudal axis of the nucleus. Calretinin (CR)-labeled somata were few and evenly distributed along the rostro-caudal axis. PV and CB distribution in the visual cortex was characterized by larger round and multipolar cells for PV, and more bitufted neurons for CB. The staining pattern for PV was the opposite of that of CR, which showed densely stained but rare cell bodies.

Tractography shows the existence of connections with the caudal visual cortex. However, we detected no contralateral projection in the visuo-claustral interconnections. Since sheep and goats have laterally placed eyes and a limited binocular vision, the absence of contralateral projections could be of prime importance if confirmed by other studies, to rule out the role of the claustrum in stereopsis.

1 | INTRODUCTION

The claustrum (Cl) is a subcortical structure, relaying inputs from, to, and among cortical areas (Day-Brown *et al*., 2016; Reser *et al*., 2017; Wang *et al*., 2017; White and Mathur, 2018; Krimmel *et al*., 2019; Jackson *et al*., 2020), including a rather large connection to and from visual areas (Norita, 1977; Riche and Lanoir, 1978; Olson and Graybiel, 1980; LeVay and Sherk, 1981; Maçarico da Costa *et al*., 2010). Other data suggest also inputs from serotonergic raphe nuclei (Baizer, 2001), thalamic nuclei (LeVay and Sherk, 1981; Carey and Neal, 1986; Vertes and Hoover, 2008), endopiriform nucleus (Lipowska *et al*., 2000), and dopaminergic neurons of the ventral tegmental area or *substantia nigra* (Pirone *et al*., 2018).

Despite the wealth of data from various species on general anatomy, cytoarchitecture, and chemoarchitecture, the structure, function, and origin of the Cl are still a matter of debate (Edelstein and Denaro, 2004; Crick and Koch, 2005; Pirone *et al*., 2012; Mathur, 2014; Hinova-Palova *et al*., 2014a, 2014b; Deutch and Mathur, 2015; Goll *et al*., 2015; Binks *et al*., 2019; Hinova-Palova *et al*., 2019a, 2019b; Pirone *et al*., 2020). To this effect, the ontology of the claustro-insular complex is still subject to debate (for in-depth discussion see Butler *et al*., 2011; Pirone *et al*., 2012), but homologies reaching birds and even reptiles have been put forward (Puelles *et al*., 2016; Watson and Puelles, 2017).

An important step in understanding the Cl function is to clarify the neurochemistry of the nucleus and identify its reciprocal connections with other brain areas. Efforts are now increasingly drawn toward precising these connections. As an example, here, we mention that there has been no knowledge of direct connection of the Cl to the non-visual thalamus (Carey and Neal, 1986; Day-Brown *et al*., 2016), until fairly recently (Atlan *et al*., 2018; Narikiyo *et al*., 2020).

The Cl contains several types of interneurons, characterized neurochemically by the presence of calcium-binding proteins (CBPs), nNOS, the synthetic enzyme for nitric oxide, and different

Andrea Pirone and Jean-Marie Graïc contributed equally to the article.

neuropeptides (Eiden *et al*., 1990; Kowiański *et al*., 2008; Hinova-Palova *et al*., 2008, 2012; Cozzi *et al*., 2014; Pirone *et al*., 2014; Landzhov *et al*., 2017). On the contrary, the presence of projecting neurons in the CI is still open. It is well-known that CBPs are classically expressed by GABA-ergic interneurons, but they have also been found in projecting neurons of different brain structures (Gerfen *et al*., 1985; Celio, 1990; Bennett-Clarke *et al*., 1992; Rausell *et al*., 1992; Baizer *et al*., 2011; Liu *et al*., 2014; Shang *et al*., 2019). This implies that some of the CBP-containing neurons in the CI may indeed project to other brain structures.

The visual cortex of the sheep has been relatively well studied compared to other ungulates. Rose (1942) found that the striated cortex stretched along most of the lateral and entolateral sulcus. Later electrophysiological studies pointed out to a much smaller dorso-occipital part of the sheep cortex (Clarke and Whitteridge, 1976; Clarke, *et al*., 1976), whereas thalamo-cortical tracing studies confirmed a wider visual territory (Karamanlidis *et al*., 1979).

One of the now often used investigation techniques involves the mapping of probabilistic tracts using diffusion tensor imaging (DTI), which has recently led a group to push for the establishment of a claustro-cortical fan (Fernández-Miranda *et al*., 2008a, 2008b). In the present study, we focused on the connections of the CI with the primary visual cortex (V1), using the sheep, a large-brained mammals often used in translational research, as experimental model, and a combination of DTI and neurochemistry as working methodology.

2 | MATERIALS AND METHODS

2.1 | Animals and tissue sampling

For the present study, we utilized the brains of six adult sheep collected at a local slaughterhouse (Table 1). Animals were treated according to the European Community Council directive (86/609/EEC) concerning animal welfare during the commercial slaughtering process and were constantly monitored under mandatory official veterinary medical care.

The ovine brains were extracted within 15 min after death and cut into transverse blocks (0.5 cm thick) containing the CL and the adjoining structures in their rostro-caudal extent. Blocks from the right hemisphere were fixed by immersion in 4% paraformaldehyde in 0.1 M phosphate-buffered saline at pH 7.4 (PBS) and later processed for paraffin embedding. Simultaneously, blocks of the left primary visual cortex were sampled across the splenial and endolateral sulcus.

TABLE 1 Specimen data

Age	Weight	Sex	Breed
Adult (4 years)	34	F	Brogna
Adult (4 years)	47	F	Brogna
Adult (4 years)	35.5	F	Brogna
Adult (4 years)	43.5	F	Brogna
Adult (4 years)	38	F	Brogna
Adult (4 years)	41	F	Brogna

2.2 | Histology and Immunohistochemistry

MRI images and coronal blocks of sheep brain, later sectioned and stained with cresyl-violet, were used to determine the shape and extent of the CI.

Immunoperoxidase reaction was performed on serial paraffin sections (5 μm) from four brain blocks representing the CI rostro-caudal extent (Figure 1). Immunoreaction was carried out employing the following antibodies against three CBPs: a mouse monoclonal anti-parvalbumin (PV, 1:2000, Sigma), a mouse monoclonal anti-parvalbumin (PV, 1:2000, Swant), a mouse monoclonal anti-calbindin D-28 K (CB, 1:2000, Sigma), a rabbit polyclonal anti-calbindin D-28 K (CB, 1:1000, Swant), a rabbit polyclonal anti-calretinin (CR, 1:100, Abcam), and a rabbit anti-calretinin (CR, 1:1000, Swant) (details are reported in Table 2). Epitope retrieval was carried out at 120°C in a pressure cooker for 3 min with a Tris/EDTA buffer, pH 9.0. Sections were pretreated with 1% H_2O_2 in PBS, for 10 min to quench endogenous peroxidase activity, then rinsed with 0.05% Triton-X (TX)-100 in PBS (3 × 10 min), and blocked for 1 hr with 5% normal horse serum (PK-7200, Vector Labs) in PBS. Serial sections were incubated overnight at 4°C in a solution containing the anti-PV or anti-CB or anti-CR with 2% normal horse serum, 0.05% TX-100 in PBS. Sections were then rinsed in PBS (3 × 10 min), followed by incubation with biotinylated anti-mouse IgG (5 μg/ml, Vector Labs, Burlingame, CA) or with biotinylated anti-rabbit IgG (5 μg/ml, Vector Labs) (details are reported in Table 3) and then with ABC reagent (Vectastain Kit, PK-7200, Vector Labs). Sections were again rinsed in PBS, for 3 × 10 min. Staining was visualized by incubating the sections in diaminobenzidine (sk-4,105, Vector Labs) solution. The negative controls were performed by replacing either the primary antibodies, anti-mouse/rabbit IgG, or the ABC complex with PBS or non-immune serum. Under these conditions, staining was abolished. Besides, positive controls were carried out testing the primaries antibodies on mouse brain sections. In addition, specificity of the antibodies had already been tested in previous studies (RRID code Tables 2 and 3).

2.3 | Image acquisition and processing

The stained sections were digitalized using a semi-automated system (D-Sight2, Menarini Diagnistics) at a magnification of 20 times.

2.4 | Tractography

MRI scans were obtained from the University of Verona with a Bruker tomograph (Bruker) equipped with a 4.7 T, 33-cm bore horizontal magnet (Oxford Ltd.). Images were acquired with a single-coil configuration. A 7.2 cm inner diameter volume birdcage coil was used as

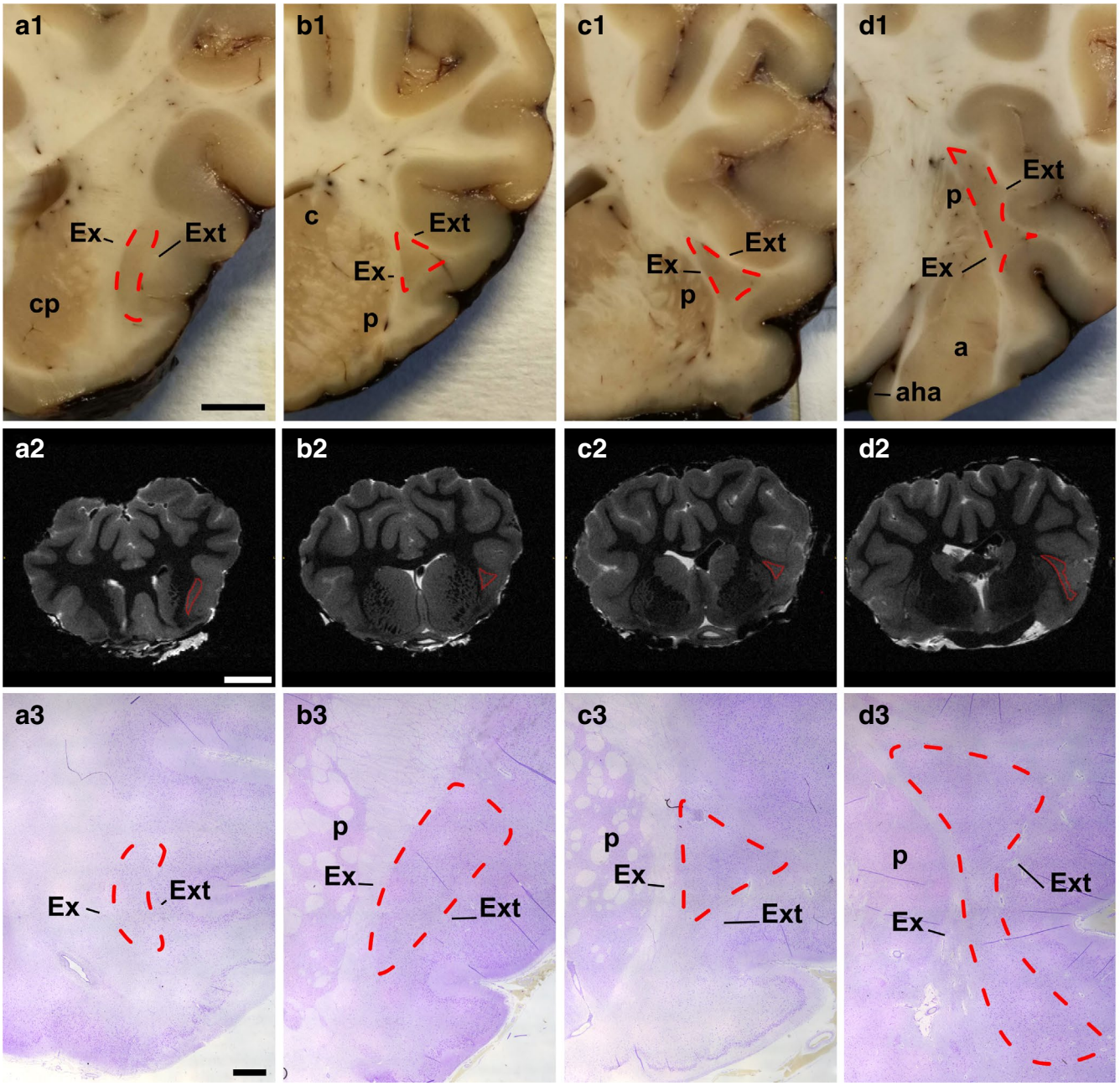

FIGURE 1 Anterior (a) to posterior (d) coronal aspects of the sheep claustrum. Fresh coronal blocks (first row a1 to d1; scale bar =5 mm); MRI digital sections (second row, scale bar =1 cm); Cresyl-violet staining (third row; scale bar =2 mm). Cl (cl) outline is drawn by red lines. a, amygdala; aha, amygdalohippocampal area; c, caudate; cp, caudoputamen; Ex, external capsule; Ext, extreme capsule; p, putamen

transmitter and receiver. Using a 2D rapid acquisition with relaxation enhancement (RARE) sequence, high-resolution T2w structural images were acquired. Parameters were as follows: repetition time (TR) 35,736 ms; echo time (TE) 78.1 ms; field of view (FOV) 6.0 × 5.0 cm; matrix size (MTX) 240 × 200; 0.250 × 0.250 mm resolution, n. slices 160, 0.5 mm thickness; RARE factor 16; number of averages (NEX) 8; and total acquisition time 1 hr and 11 min. Diffusion tensor images were acquired with an echo planar imaging (EPI) sequence. Parameters were as follows: TR 20,000 ms, TE 24.7 ms, FOV 6.0 × 5.0 cm; MTX 120 × 100; isotropic in-plane resolution of 0.5 mm; slice thickness 1.0 mm; n. slice 80; EPI factor 11; NEX 6; 30 noncollinear directions acquired with a b-value of 3000 s/mm^2 and 5 b0 images for a total acquisition time of about 12 hr 50 min.

A DTI diffusion scheme was used, and a total of 30 diffusion sampling directions were acquired. The *b*-value was 3,000 s/mm^2, with a voxel size of 0.5 × 0.5 × 1 mm. We used then DSI Studio (http://dsi-studio.labsolver.org) for the tractography analysis. After computing the diffusion tensor, a deterministic fiber tracking algorithm (Yeh *et al.*, 2013) was used. Ending regions were placed at the right Cl with a volume size of 7e+02 mm^2 and left Cl with a volume size of 6.5e+02 mm^2. A seeding region was placed in the right primary visual cortex with a volume size of 4.1e03 mm^2 and the left primary visual cortex with a

TABLE 2 Primary antibodies

Antibody	Immunogen	Manufacturing details	Dilution
Anti-PV	PARV-19 hybridoma produced by the fusion of mouse myeloma cells and splenocytes from an immunized mouse. Purified frog muscle parvalbumin was used as the immunogen	Sigma-Aldrich, mouse monoclonal, Clone PARV-19, Product No. P 3088 RRID: AB_477329	1:2000
Anti-PV	Produced by hybridization of mouse myeloma cells with spleen cells from mice immunized with parvalbumin purified from carp muscles	Swant, mouse monoclonal, Code No: 235, Lot no: 10-11 (F) RRID: AB_10000343	1:2000
Anti-CR	The antibody against calretinin was produced in mice by immunization with recombinant human calretinin−22 k (identical with calretinin up to Arg178 N-terminal)	Swant, mouse monoclonal, Cat# 6B3, Lot n° 010399 RRID: AB_10000320	1:1000
Anti-CR	Full length protein	Abcam, rabbit polyclonal, ab702 RRID: AB_305702	1:100
Anti-CB	Derived from the CB-955 hybridoma produced by the fusion of mouse myeloma cells and splenocytes from BALB/c mice immunized with a purified bovine kidney calbindin-D-28 K	Sigma-Aldrich, mouse monoclonal, Clone CB−955, C9848 RRID: AB_476894	1:2000
Anti-CB	This antiserum was produced against recombinant rat calbindin D-28 K (CB)	Swant, rabbit polyclonal, Lot No.: 9.03, Code No.: CB−38a RRID: AB_10000340	1:1000

TABLE 3 Secondary antibodies

Antibody	Type	Manufacturing details	Dilution (μg/ml)
Biotinylated	Anti-mouse IgG (H + L)	Vector Labs, Burlingame, horse, Cat.n. BA-2001, Lot.n. ZC1230 RRID: AB_2336180	5
Biotinylated	Anti-rabbit IgG (H + L)	Vector Labs, Burlingame, horse, Cat.n. BA−1100, Lot.n. ZA0319 RRID: AB_2336201	5

volume size of 4.2e03 mm^2. The anisotropy threshold was 0.05896. The angular threshold was 45°. The step size was 0.1 mm. The fiber trajectories were smoothed by averaging the propagation direction with 50% of the previous direction. Tracks with length shorter than 2 or longer than 200 mm were discarded. A total of 50,000 seeds were placed.

Identification of the presented tracts was achieved by segmenting by hand the visual cortical region, chosen as origin, and the CI area as the end region, and calculating the white matter tracts running between them. Anatomical references were found in historical papers and recent atlases (Clarke and Whitteridge, 1976; Vanderwolf and Cooley, 2002; Nitzsche *et al.*, 2015).

3 | RESULTS

3.1 | Claustrum overview

The rod-like shaped CI was identified in the ventrolateral telencephalon in the series of rostral coronal blocks, MRI images and in cresyl-violet stained sections (Figure 1 (a1–a3)). The nucleus then assumed a triangular aspect in the middle region (Figure 1 (b1-b3, c1-c3), Figure 2). In the caudalmost region, dorsolateral to the amygdala, the

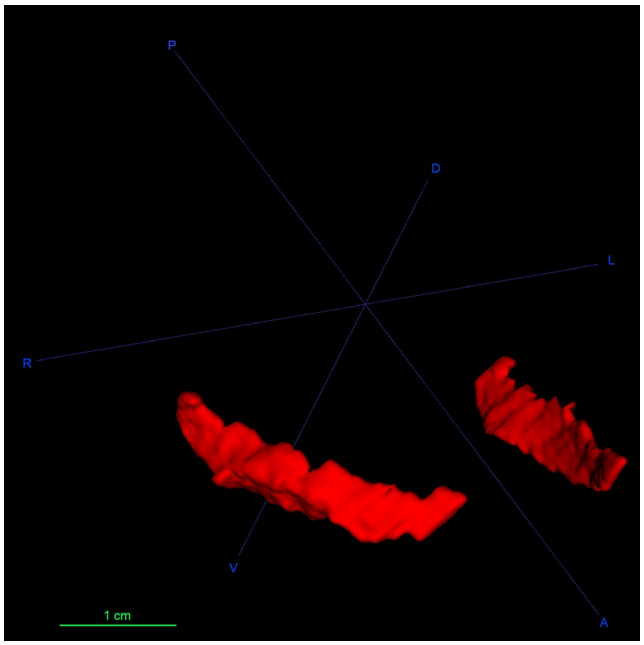

FIGURE 2 3D reconstruction of the sheep claustrum in red. A, anterior; D, dorsal; L, left; P, posterior; R, right; V, ventral

Cl was characterized by a larger and irregular area (Figure 1 (d1-d3)). Cl was encased in the white matter of the external (Ex) and extreme (Ext) capsules.

3.2 | Immunohistochemistry

Two different antibodies for each CBP were employed and each pair, with the exception of CB, gave the same results. Monoclonal antibody against CB gave negative results both in the Cl and in the visual areas, but clearly stained the Purkinje neurons of the sheep cerebellum (see Figure 1, Video S1). Differently, polyclonal anti-CB immunoreaction was observed both in visual cortex and in Cl.

3.2.1 | Claustrum

Immunoperoxidase staining in the sheep Cl revealed the presence of both cell bodies and fibers positive to PV, CR, and CB (Figure 3). CR immunoreactivity was evenly distributed throughout the dorsoventral and rostro-caudal extent of the CL, while PV and CB stained somata increased moving toward the caudal region. The semi-quantitative representation of the PV, CR, and CB immunostaining distribution is reported in Table 4.

Positive fibers were seen running in all directions throughout the rostro-caudal and the dorsoventral extent of the CL with a homogeneous distribution. In particular, PV and CB immunoreactive (-ir) fibers were scarce (Figure 3(a–d)), while CR-positive fibers made up a dense network surrounding negative cell bodies (Figure 3(e)).

3.2.2 | Visual area

The visual area of the ovine cortex was identified based on the available stereotaxic atlases of the species (Richard, 1967; Vanderwolf and Cooley, 2002; Nitzsche *et al*., 2015) and relevant literature (Rose, 1942; Clarke and Whitteridge, 1976; Clarke *et al*., 1976; Karamanlidis *et al*., 1979). The immunocytochemistry of the visual area in the sheep caudal cortex around the lateral sulcus identified largely different GABA-ergic interneuron populations within the cortical thickness (Figure 4).

Calbindin-ir was distributed mostly among layer 3–6 (Figure 4(e)) with a diffuse band of fibers across the layer 3–5 border. Larger somata were present in layer 5, and bipolar bitufted cells were seen in layer 3. Some pyramidal cells were positive to CB immunostaining (Figure 4(f)). Monoclonal anti-CB did not provide satisfactory staining.

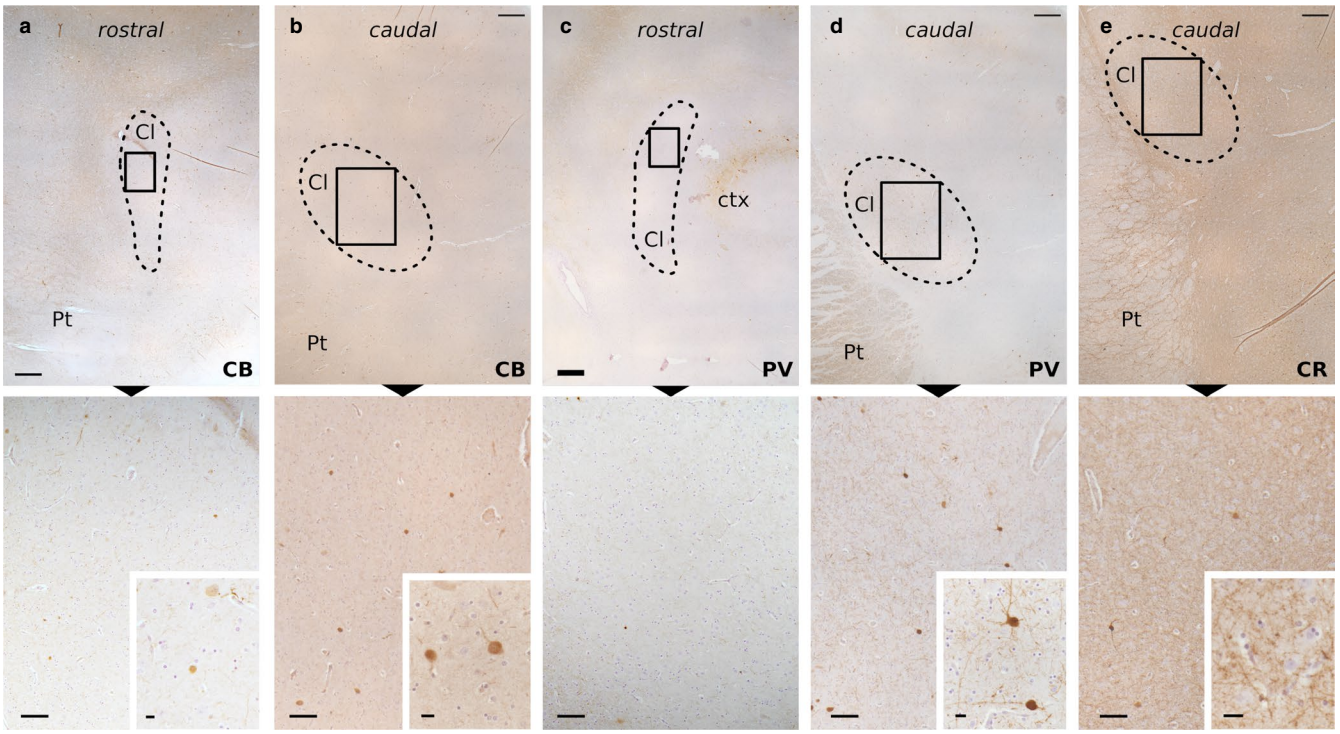

FIGURE 3 Immunohistochemical staining of the sheep Cl. Immunoperoxidase reaction shows the distribution of CB in the rostral (a) and caudal (b) parts, PV in the rostral (c) and caudal (d) parts, and CR caudal part (e) immunoreactivity in the Cl (dashed line). Below (a), very few and weakly stained CB-ir cells are spotted. Higher magnification of the frames below (b) displays CB-ir cells and scarce fibers (enlarged in the inset). Below (c) are rare fibers with no real soma stain for PV. Below (d), higher magnification shows a moderate density of PV-ir fibers and two positive neurons (enlarged in the inset). Below (e), higher magnification shows a dense network of CR-positive fibers (enlarged in the inset). Cl, claustrum; ctx, cortex; Pt, putamen. Scale bars =500 μm (upper row), 100 μm (lower row), 10 μm (insets)

TABLE 4 Semi-quantitative representation of PV, CR, and CB-ir somata throughout the rostro-caudal levels (A most rostral, D most caudal) of the CI. –, 0 somata; +, 1–20 somata; ++, 21–40 somata; +++, 41–60 somata; ++++, 61–80 somata

Levels	PV	CR	CB
A	–	+	+
B	++	+	++
C	+++	+	+++
D	++++	+	+++

Calretinin-ir neurons were scarce in the V1 area, in which they were found in layer 3 with some also present in layer 5. An extensive neuropil web covered all of the cortical thickness with predominant bands in upper layer 1 and mid-layer 5 (Figure 4(h,i)). An even clearer fiber band pattern was present in the adjacent peristriate area.

Parvalbumin was very clearly marking layer 3–6 with large round somata with vertically oriented dendrites. There were seemingly slightly more cell bodies within layer 5 (Figure 4(k)). A broad band corresponding to the layer 3–5 border was a major feature of V1. The peristriate area showed no staining (Figure 4(c,j,k)). Weak positivity

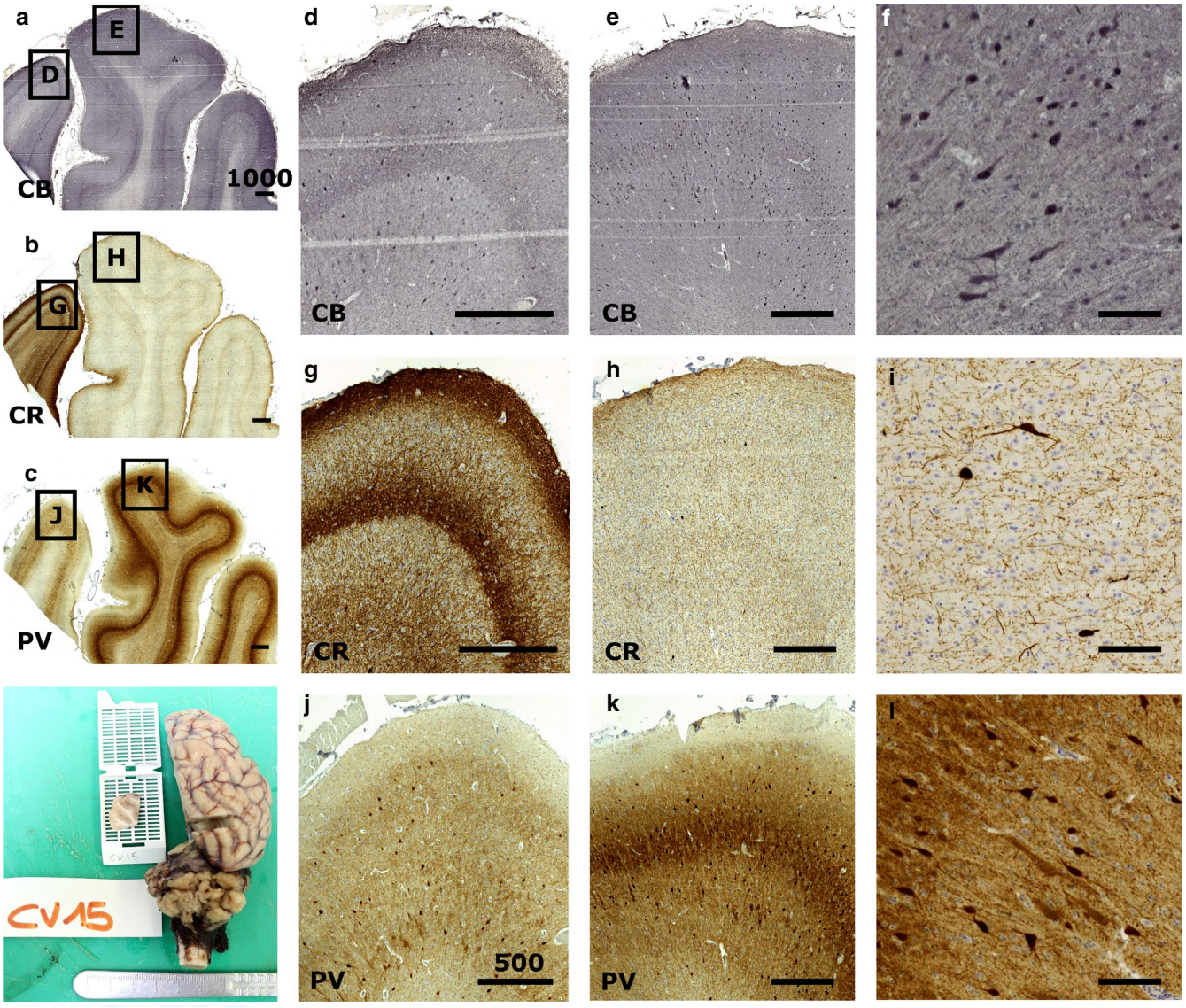

FIGURE 4 Immunocytochemical staining of the sheep V1. Immunocytochemistry reveals the patterns of calcium-binding proteins in V1 (e, h, k) and the peristriate area (d, g, j). Calbindin is found in most of the cortical thickness (a, d, e, f), staining round interneurons and some pyramidal cells, while calretinin is much more localized, notably in layer 1 (b, g, h, i). Parvalbumin shows also a large positivity throughout the cortical thickness (c, j, k, l) with a marked neuropil band in V1 (k). Positive cells are rather large and round multipolar, with weaker staining of some pyramidal neurons (l). Bar in (a), (b), (c) is 1000 μm; bar in (d), (e), (g), (h), (j), and (k) is 500 μm, (f), (i), (l) bar is 50 μm

could be seen on some pyramidal cells that could be attributed to dendritic synapsing with PV-ir cells covering the pyramidal somata or to a markedly lower amount of PV (Figure 4(l)).

3.3 | Tractography

The tractography algorithm computed between the CI area and the wider visual cortical area elicited robust fiber tracts following an ipsilateral course (Figure 5). Tracts running directly to the CI emerged from the occipital end of the visual cortical sensory area (Figure 5a) through a quite homogeneous bundle, traveling along the optic radiation and going through the external capsule region, to reach the claustral territory. Few fibers reached further in the frontal part of the sheep cortex. Despite a large V1 delimitation, only a dorsolateral, occipital band of fibers were found to reach for the CI. Seeding from the CI caused the appearance of additional connection tracts between the caudal part of the CI to the rostral end of the visual area, toward the rostral end of the marginal sulcus (Figure 5). Although tract endings are not the *forte* of tractography, the tracts reaching the CI seemed not to end at the dorsocaudal entry from the external capsule, but continue further into the anterior claustral area. We could not find any reliable commissural innervation from V1 to the CI, while V1-V1 commissural fibers could be detected (not shown).

4 | DISCUSSION

In the present study, we have analyzed different neuronal populations in both the CI and the visual cortex of the sheep, based on the patterns of CBPs expression. We also defined the fiber tracts running between the left and right CI and the visual areas by MRI scans.

4.1 | Choice of markers and methodology

The choice of CBPs as neurochemical markers of the CI and visual cortex is based on former studies that indicated that they represent good markers for both structures (for general references see Glezer *et al*., 1993; Hinova-Palova *et al*., 2007; Mathur *et al*., 2009; Mathur, 2014). In particular, PV allows to distinguish the CI from the endopiriform nucleus (En) and, in fact, in our samples, it was impossible to identify the En in sections immunostained for PV. However, we cannot exclude its presence considering that it has been described in different species (marmoset: Watakabe, 2017; rat: Watson and Puelles, 2017; bat: Orman *et al*., 2017).

Our experimental series yielded also some unexpected methodological results. The monoclonal antibody anti-CB did not reveal immunoreactivity in the investigated structures, despite having been employed in countless publications (RRID: AB_476894). Here, we emphasize that the same antibody elicited a clear positivity in our

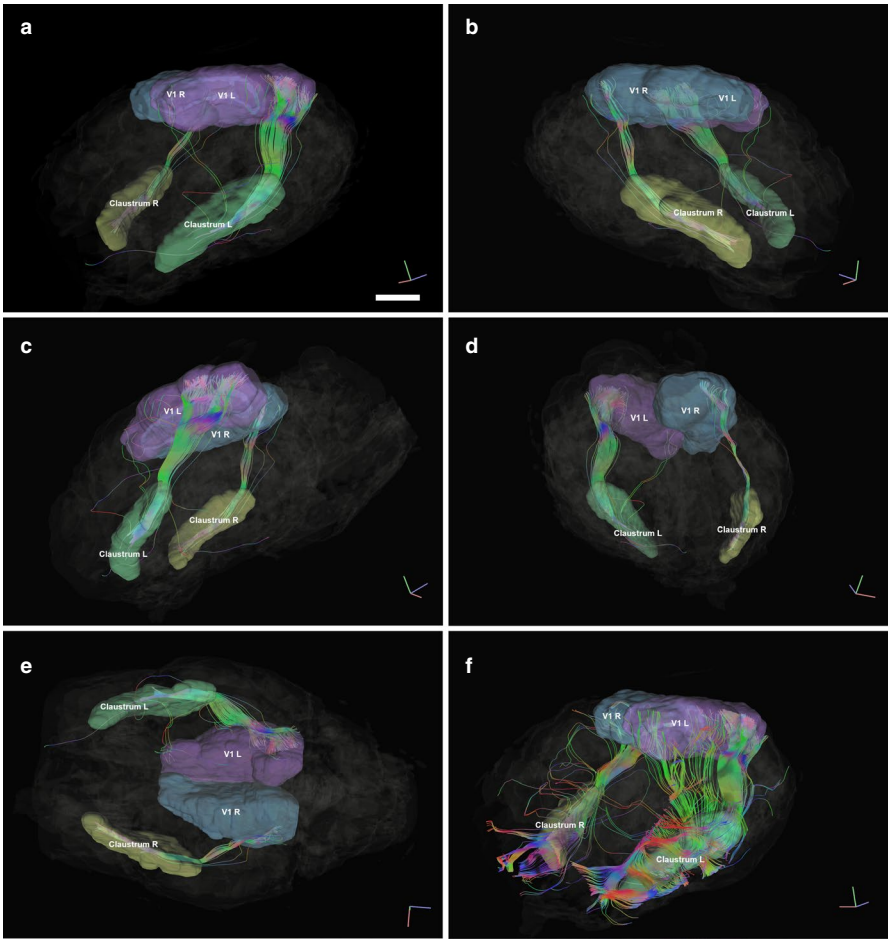

FIGURE 5 Representation of fiber tracts running between the left and right CI (yellow and red, respectively) and the left and right visual areas (in blue and green, respectively). MRI images represent the orthogonal planes. (a) Left antero-lateral view. Indicative bar = 1 cm. (b) Right antero-lateral view. In (a) and (b), the extent of the tracts in the claustra can be appreciated, as well as the posterior access of the fibers, originating from the occipital aspect of the visual cortex. (c) Left Lateral view. (d) Right postero-lateral view. (e) Ventral view where the left tracts can be seen reaching up to the visual cortex in the dorso-occipital cortex. (f) Left antero-lateral view, where the CI is used as a seed to map the tracts originating from it. The fibers exiting the CI are very rich. Note the projection to the anterior part of the visual territory, emerging from the caudo-dorsal part of the CI

positive control, represented by cerebellar Purkinje cells (see Video S1). One possible explanation might be that there are two different forms of calbindin in the sheep, with a differential expression in the neocortex and the cerebellum, both marked by our polyclonal antibody. And indeed, it is worth noting that in *Ovis aries*, two calbindin CALB1 and CALB2, of 262 aa and 271 aa, respectively, are described (UniProt). Further investigations are needed to shed light on this scenario, in particular ascribing to the precise antibody target.

4.2 | Claustrum

Our samples showed the unusual shape of the sheep Cl. Indeed, it did not resemble any scheme of Cl type described by Kowianski *et al.* (1999); however, the shape we observed in the rostral and medial sections was similar to that described in the pig (Pirone *et al.*, 2019). Moreover, the triangular aspect of the middle sheep Cl was a feature found in zebras, lamas, and zebus (Buchanan and Johnson, 2011), and also in cats even if the dorsal triangular cat Cl extends ventrally with a thin stem (Sherk, 1986; Johnson *et al.*, 2014).

In our sections and in the 3D model (Figure 2), the sheep Cl appeared as a continuous structure, in contrast from what was reported for the Cl in the gorilla, cetaceans, and pigs, where cell islands or lobulations were described (Baizer *et al.*, 2014; Johnson *et al.*, 2014; Pirone *et al.*, 2020). As in other mammal species, the sheep Cl was encased in an external and extreme capsule, the latter lacking or being poorly developed in *Insectivora* and in some rodents (Kowianski *et al.*, 1999); these two capsules make the Cl easily distinguishable from its surrounding structures.

Immunoperoxidase investigation revealed a particular distribution pattern of PV, CR, and CB within the sheep Cl. The semi-quantitative representation of CBPs immunoreactive somata showed that PV and CB-positive cell bodies increased, moving caudally. Our data show that CR-labeled somata were few and evenly distributed along the rostro-caudal axis, contrarily to what reported for marine Cetartiodactyls, were CR-containing neurons were prevalent in the Cl (Cozzi *et al.*, 2014). Furthermore, PV and CB-ir fibers were scarce while CR-positive fibers formed a dense network surrounding negative cell bodies.

CBPs immunoreactivity was seen throughout the Cl of other mammal species (rat: Druga *et al.*, 1993; monkey: Reynhout and Baizer, 1999; cat: Hinova-Palova *et al.*, 2007; Rahman and Baizer, 2007; human: Hinova-Palova *et al.*, 2014; human, chimpanzee, macaque: Pirone *et al.*, 2014; dog: Pirone *et al.*, 2015; squirrel monkey: Baizer *et al.*, 2020), suggesting that similar subclasses of Cl neurons exist in multiple species and share a homogeneous spatial distribution pattern throughout the anterior–posterior extent of the Cl.

The distribution of CBPs immunoreactivity is not homogeneous along the dorsal–ventral axis of the Cl. In the human Cl, there are more PV-ir elements in the central portion of the nucleus than in the dorsal and ventral aspects (Hinova-Palova *et al.*, 2014). In the cat and dog, the superior Cl contains a higher number of PV-ir somata, and the quantity progressively decreases in the intermediate and inferior parts (Hinova-Palova *et al.*, 2007; Pirone *et al.*, 2015). In human, chimpanzee and macaque Cl both CR- and PV-ir neurons are mostly localized in the central and ventral region of the structure (Pirone *et al.*, 2014). Dorsoventral subdivisions of the Cl are important, as the dorsal Cl is the part connected to the visual cortex in the cat (LeVay and Sherk, 1981; Minciacchi *et al.*, 1995), but not in primates, where the visual Cl is in the ventral Cl (Remedios *et al.*, 2010).

Our present findings on the distribution of PV-ir cell bodies in the sheep are similar to those we have recently observed in the pig (Pirone *et al.*, 2019), another Cetartiodactyl. In both species, positive somata increased along the rostro-caudal axis of the nucleus. This pattern, considered together with that of CB, might suggest a potentially specific function of the caudal end of the sheep Cl, as already hypothesized for the pig.

4.3 | Visual cortex

The localization of CBPs has been reported in the visual cortex of several mammals, including primates and rodents (for comparative studies see Glezer *et al.*, 1993), carnivores (Yu *et al.*, 2011), bat (Kim *et al.*, 2016), and cetaceans (Hof *et al.*, 1999). However, the presence and distribution of CBPs in the visual cortex of hoofed mammals is seldom reported (Hof *et al.*, 1999) and reflects the reduction of the isocortex to five layers (for general discussion see Cozzi *et al.*, 2017; for the sheep see Peruffo *et al.*, 2019). In our experimental series, we found many multipolar and fusiform CB-ir neurons diffuse through the lower layers of the cortex, but not in layer 1, 2, and the upper part of layer 3. The low density of intensely stained CR-ir neurons in our preparations does not reflect the accepted view that the number of CR-positive neurons is much higher than that of CB-positive neurons (Hof *et al.*, 1999). The CR-ir neurons present in layer 2, 3, and 5 were, however, relatively large, and their pattern was comparable to what was found in other hoofed mammals as the camel (Hof *et al.*, 1999).

Interestingly, we noted that in the sheep, the staining pattern for PV was the opposite of that for CR, which showed a marked stain in the medially adjacent gyrus (cingulate, see Figure 4). Our data present some difference with what described on the distribution and relative presence of CPBs in Cetardiodactyls by Hof et al. in their seminal paper (Hof *et al.*, 1999), to which we refer for comparison. A weak staining of pyramidal cells for CB in layer 3 has been reported previously (Hof *et al.*, 1999), and here, we report that PV staining in pyramidal layer 3 is weak too (Figure 4). This points out to the relative similarity in PV and CB distribution, characterized by larger round and multipolar cells for PV, and more bitufted neurons for CB (Figure 4). Interestingly, the staining pattern for PV was the opposite of that of CR, which showed a marked stain in the medially adjacent gyrus (cingulate, see Figure 4).

Neurons expressing CBPs are classically considered GABA-ergic interneurons mainly localized in the neocortex (see Tremblay *et al.*, 2016 for review). Long-range GABA-ergic neurons have been shown to project in cortico-cortical bundles, and in bidirectional

hippocampo-entorhinal reciprocal inhibition (Tomioka and Rockland, 2007; Melzer *et al*., 2012). However, CBPs have also been spotted in projections outside the prosencephalon. PV and CB have been reported in the *substantia nigra*, trigeminal nucleus, and in thalamic neurons that project to the cortex (Gerfen *et al*., 1985; Bennett-Clarke *et al*., 1992; Rausell *et al*., 1992), while CR has been found to be dynamically expressed in L5a excitatory pyramidal neurons of the mouse barrel cortex (Liu *et al*., 2014). Recently, PV-positive excitatory neurons have been identified in the superior colliculus of the mouse, their projections making up the visual pathway to trigger fear (Shang *et al*., 2019). Moreover, projection neurons of the inferior olive express both CR and CB (Baizer *et al*., 2011) and the Purkinje cells of the cerebellar cortex express PV (Celio, 1990). Substantiated connections seem to exist in primates (Tanné-Gariépy *et al*., 2002; Fernàndez-Miranda *et al*., 2008), cats (LeVay and Sherk, 1981), rabbits (Carman *et al*., 1964; Gutierrez-Ibarluzea *et al*., 1999), and sheep, and the CI itself activates during visuomotor tasks and integration (Baugh *et al*., 2011). However, spineless neurons in both in the claustrum and the visual cortex of the cat have been shown to be non-projecting neurons (LeVay and Sherk, 1981). In rabbits, retrograde tracing seemed to demonstrate direct connections from Brodmann's area 17 by pyramidal cells and stellate cells (Gutierrez-Ibarluzea *et al*., 1999). Recent research reports that some claustral cells co-express VGLUT1 and GAD65, suggesting that projecting neurons in the claustrum could provide inhibition to neurons either locally or in more distant cortical areas (Atlan *et al*., 2018). Although our data does not shine light on any directionality, as a working hypothesis, we may consider that part of that input to the CI in the sheep could be inhibitory and mediated by GABA-ergic neurons.

4.4 | Tractography

Tractography has been applied to map human cortico-claustral connections and reported the presence of occipito-frontal fascicles coming from the occipito-parietal region to the CI and beyond (Fernàndez-Miranda et al., 2008; Fernández-Miranda *et al*., 2015; Meola *et al*., 2015). This is in agreement with our more focused DTI which was limited to the primary visual area in the dorso-occipital region of the sheep brain and its connection to the CI. The emerging bundle from V1 seems to concord with Clarke and Whitterige's (1976) reduced V1 findings. Our data therefore confirm the existence of such a bundle seems in the sheep. As was shown in the mouse (Atlan *et al*., 2017), our tracts reveal a rather central, tight bundle reaching the claustrum (Figure 5). However, we detected no contralateral projection in the visuo-claustral interconnections. In all of our subjects used for tractography ($n = 3$), a slight inconstant asymmetry was observed, which could have resulted from the variability in hand parsing of the cortical areas, or specimen variability, but no anatomical feature should be deducted from it. Given the fact that the regions were segmented by hand, there is a risk to catch unrelated passing fibers, which is especially problematic in the white-matter embedded claustrum. However, this is applicable to any similar study, and we did our best to be conservative in the segmentation. A known limitation of tractography is the estimation of tract endings, and most importantly, directionality. There seems to be evidence, however, that a visual to claustrum connection exists, at least in the mouse (Wang *et al*., 2017). Finally, in the cat, the visual zone is sitting at the dorsocaudal part of the clausrtum (Sherk, 1986), which is coherent with the entry level of our tracts (Figure 5(e)).

Sheep and goats have laterally placed eyes and a limited binocular vision, but they do possess binocular neurons (Clarke and Whitteridge, 1976; Clarke *et al*., 1976) and are known to have a good depth perception (Walk and Gibson, 1961). Contralateral claustro-visual projections have long been described in the cat (Jayaraman and Updyke, 1979; Sanides and Buchholtz, 1979; Olson and Graybiel, 1980; Squatrito *et al*., 1980). We lowered the thresholds used for the ipsilateral bundles in the attempt to find crossing fibers reaching the contralateral CI, but with no result. Our data suggest that contralateral connections are absent in the sheep, or perhaps very limited as in the cat (Olson and Graybiel, 1980). We also note that connections (seeding from the claustrum, Figure 5(f)) may reach peristriate areas such as V2, V3, or V4 that we did not map, because their precise location and topography has not been identified in the sheep, although tracing studies showed a quite wide visual territory (Karamanlidis *et al*., 1979). The absence of contralateral projections could be of prime importance if confirmed by other studies, to rule out the role of the CI in stereopsis.

ACKNOWLEDGEMENTS

The authors would like to thank Dr. Giuseppe Palmisano and Giovanni Caporale from the University of Padova for their technical help.

CONFLICT OF INTEREST

The authors declare no conflict of interest.

DATA AVAILABILITY STATEMENT

The data that support the findings of this study are available from the corresponding author upon reasonable request.

ORCID

Andrea Pirone https://orcid.org/0000-0001-6363-392X
Jean-Marie Graïc https://orcid.org/0000-0002-1974-8356
Enrico Grisan https://orcid.org/0000-0002-7365-5652
Bruno Cozzi https://orcid.org/0000-0002-7531-7040

REFERENCES

Atlan, G., Terem, A., Peretz-Rivlin, N., Groysman, M. & Citri, A. (2017) Mapping synaptic cortico-claustral connectivity in the mouse. *The Journal of Comparative Neurology*, 525, 1381–1402. https://doi.org/10.1002/cne.23997

Atlan, G., Terem, A., Peretz-Rivlin, N., Sehrawat, K., Gonzales, B.J., Pozner, G. *et al.* (2018) The Claustrum supports resilience to distraction. *Current Biology*, 28(17), 2752–2762.e7. https://doi.org/10.1016/j.cub.2018.06.068

Baizer, J.S. (2001) Serotonergic innervation of the primate claustrum. *Brain Research Bulletin*, 55, 431–434.

Baizer, J.S., Webster, C.J. & Baker, J.F. (2020) The Claustrum in the squirrel monkey. *Anatomical Record*, 303, 1439–1454.

Baizer, J.S., Sherwood, C.C., Hof, P.R., Witelson, S.F. & Sultan, F. (2011) Neurochemical and structural organization of the principal nucleus of the inferior olive in the human. *Anatomical Record (Hoboken)*, 294, 1198–1216.

Baizer, J.S., Sherwood, C.C., Noonan, M. & Hof, P.R. (2014) Comparative organization of the claustrum: what does structure tell us about function? *Frontiers in Systems Neuroscience*, 2(8), 117. 0.3389/fnsys.2014.00117

Baugh, L.A., Lawrence, J.M. & Marotta, J.J. (2011) Novel claustrum activation observed during a visuomotor adaptation task using a viewing window paradigm. *Behavioural Brain Research*, 223(2), 395–402.

Bennett-Clarke, C.A., Chiaia, N.L., Jacquin, M.F. & Rhoades, R.W. (1992) Parvalbumin and calbindin immunocytochemistry reveal functionally distinct cell groups and vibrissa-related patterns in the trigeminal brainstem complex of the adult rat. *The Journal of Comparative Neurology*, 320, 323–338.

Binks, D., Watson, C. & Puelles, L. (2019) A re-evaluation of the anatomy of the claustrum in rodents and primates—analyzing the effect of pallial expansion. *Frontiers in Neuroanatomy*, 13, 34.

Buchanan, K.J. & Johnson, J.I. 2011. Diversity of spatial relationships of the claustrum and insula in branches of the mammalian radiation. *Annals of the New York Academy of Sciences*, 1225(Supp. 1), E30–E63. https://doi.org/10.1111/j.1749-6632.2011.06022.x

Butler, A.B., Reiner, A. & Karten, H.J. (2011) Evolution of the amniote pallium and the origins of mammalian neocortex. *Annals of the New York Academy of Sciences*, 1225, 14–27. https://doi.org/10.1111/j.1749-6632.2011.06006.x

Carey, R.G. & Neal, T.L. (1986) Reciprocal connections between the claustrum and visual thalamus in the tree shrew (*Tupaia glis*). *Brain Research*, 386, 155–168.

Carman, J.B., Cowan, W.M. & Powell, T.P. (1964) the Cortical Projection Upon the Claustrum. *Journal of Neurology, Neurosurgery and Psychiatry*, 27, 46–51. https://doi.org/10.1136/jnnp.27.1.46

Celio, M.R. (1990) Calbindin D-28k and parvalbumin in the rat nervous system. *Neuroscience*, 35, 375–475.

Clarke, P.G.H. & Whitteridge, D. (1976) The cortical visual areas of the sheep. *Journal of Physiology*, 256, 497–508. https://doi.org/10.1113/jphysiol.1976.sp011335

Clarke, P.G.H., Donaidson, I.M.L. & Whitteridge, D. (1976) Binocular visual mechanisms in cortical areas I and II of the sheep. *The Journal of Physiology*, 256, 509–526.

Cozzi, B., Roncon, G., Granato, A., Giurisato, M., Castagna, M., Peruffo, A. *et al.* (2014) The claustrum of the bottlenose dolphin Tursiops truncatus (Montagu 1821). *Frontiers in Systems Neuroscience*, 8, 42. https://doi.org/10.3389/fnsys.2014.00042

Cozzi, B., De Giorgio, A., Peruffo, A., Montelli, S., Panin, M., Bombardi, C. *et al.* (2017) The laminar organization of the motor cortex in monodactylous mammals: a comparative assessment based on horse, chimpanzee, and macaque. *Brain Struct Funct*, 222, 2743–2757. https://doi.org/10.1007/s00429-017-1397-z

Crick, F.C. & Koch, C. (2005) What is the function of the claustrum? *Philosophical Transactions of the Royal Society B: Biological Sciences*, 360, 1271–1279. https://doi.org/10.1098/rstb.2005.1661

Day-Brown, J.D., Slusarczyk, A.S., Zhou, N., Quiggins, R., Petry, H.M. & Bickford, M.E. (2016) Synaptic organization of striate cortex projections in the tree shrew: a comparison of the claustrum and dorsal thalamus. *The Journal of Comparative Neurology*, 52, 1403–1420.

Deutch, A.Y. & Mathur, B.N. (2015) Editorial: the CL: charting a way forward for the brain's most mysterious nucleus. *Frontiers in Systems Neuroscience*, 9, 103.

Druga, R., Chen, S. & Bentivoglio, M. (1993) Parvalbumin and calbindin in the rat claustrum: an immunocytochemical study combined with retrograde tracing frontoparietal cortex. *Journal of Chemical Neuroanatomy*, 6, 399–406.

Edelstein, L.R. & Denaro, F.J. (2004) The claustrum: a historical review of its anatomy, physiology, cytochemistry and functional significance. *Cellular and Molecular Biology*, 50, 675–702.

Eiden, L.E., Mezey, E., Eskay, R.L., Beinfeld, M.C. & Palkovits, M. (1990) Neuropeptide content and connectivity of the rat claustrum. *Brain Research*, 523, 245–250.

Fernández-Miranda, J.C., Rhoton, A.L., Álvarez-Linera, J., Kakizawa, Y., Choi, C. & De Oliveira, E.P. (2008) Three-dimensional microsurgical and tractographic anatomy of the white matter of the human brain. *Neurosurgery*, 62, 989–1028. https://doi.org/10.1227/01.NEU.0000297076.98175.67

Fernández-Miranda, J.C., Rhoton, A.L., Kakizawa, Y., Choi, C. & Álvarez-Linera, J. (2008) The claustrum and its projection system in the human brain: a microsurgical and tractographic anatomical study – laboratory investigation. *Journal of Neurosurgery*, 108, 764–774. https://doi.org/10.3171/JNS/2008/108/4/0764

Fernández-Miranda, J.C., Wang, Y., Pathak, S., Stefaneau, L., Verstynen, T. & Yeh, F.C. (2015) Asymmetry, connectivity, and segmentation of the arcuate fascicle in the human brain. *Brain Structure and Function*, 220, 1665–1680. https://doi.org/10.1007/s00429-014-0751-7

Gerfen, C.R., Baimbridget, K.G. & Miller, J.J. (1985) The neostriatal mosaic: compartmental distribution of calcium-binding protein and parvalbumin in the basalganglia of the rat and monkey. *Proceedings of the National Academy of Sciences of the United States of America*, 82, 8780–8784.

Glezer, I.I., Hof, P.R., Leranth, C. & Morgane, P.J. (1993) Calcium- binding protein-containing neuronal populations in mammalian visual cortex: a comparative study in whales, insectivores, bats, rodents, and primates. *Cerebral Cortex*, 3, 249–272.

Goll, Y., Atlan, G. & Citri, A. (2015) Attention: the claustrum. *Trends in Neurosciences*, 38, 486–495. https://doi.org/10.1016/j.tins.2015.05.006

Gutierrez-Ibarluzea, I., Acera-Osa, A., Mendizabal-Zubiaga, J.L., Arana-Arri, E., Bueno-Lopez, J.L., Reblet, C. *et al.* (1999) Morphology and laminar distribution of cortico-claustral neurons in different areas of the rabbit cerebral cortex. *Journal of Anatomy*, 3(2), 101–109.

Hinova-Palova, D.V., Edelstein, L.R., Paloff, A.M., Hristov, S., Papantchev, V.G. & Ovtscharoff, W.A. (2007) Parvalbumin in the cat claustrum: ultrastructure, distribution and functional implications. *Acta Histochemica*, 109, 61–77.

Hinova-Palova, D., Edelstein, L., Papantchev, V., Landzhov, B., Malinova, L., Todorova-Papantcheva, D. *et al.* (2012) Light and electron-microscopic study of leucine enkephalin immunoreactivity in the cat claustrum. *Journal of Molecular Histology*, 43, 641–649.

Hinova-Palova, D., Edelstein, L., Paloff, A., Hristov, S., Papantchev, V. & Ovtscharoff, W. (2008) Neuronal nitric oxide synthase immunopositive neurons in cat claustrum—a light and electron microscopic study. *Journal of Molecular Histology*, 39, 447–457.

Hinova-Palova, D.V., Edelstein, L., Landzhov, B., Minkov, M., Malinova, L., Hristov, S. *et al.* (2014a) Topographical distribution and morphology of NADPH-diaphorase-stained neurons in the human claustrum. *Frontiers in Systems Neuroscience*, 27(8), 96. https://doi.org/10.3389/fnsys.2014.00096

Hinova-Palova, D.V., Edelstein, L., Landzhov, B.V., Braak, E., Malinova, L.G., Minkov, M. *et al.* (2014b) Parvalbumin immunoreactive neurons in the human CL. *Brain Structure & Function*, 219, 1813–1830.

Hinova-Palova, D., Kotov, G., Landzhov, B., Edelstein, L., Iliev, A., Stanchev, S. *et al.* (2019a) Cytoarchitecture of the dorsal claustrum of the cat: a quantitative Golgi study. *Journal of Molecular Histology*, 50(5), 435–457. https://doi.org/10.1007/s10735-019-09839-7

Hinova-Palova, D., Landzhov, B., Iliev, A., Kotov, G., Stanchev, S., Kirkov, V. *et al.* (2019b) Ultrastructure of the dorsal claustrum in cat. II. Synaptic organization. *Acta Histochemica*, 121(4), 383–391. https://doi.org/10.1016/j.acthis.2019.02.009

Hof, P.R., Glezer, I.I., Condé, F., Flagg, R.A., Rubin, M.B., Nimchinsky, E.A. *et al.* (1999) Cellular distribution of the calcium-binding proteins parvalbumin, calbindin, and calretinin in the neocortex of mammals: phylogenetic and developmental patterns. *Journal of Chemical Neuroanatomy*, 16, 77–116.

Jackson, J., Smith, J.B. & Lee, K.B. (2020) The Anatomy and Physiology of Claustrum-Cortex Interactions. *Annual Review of Neuroscience*, 43, 231–247.

Jayaraman, A. & Updyke, B.V. (1979) Organization of visual cortical projections to the claustrum in the cat. *Brain Research*, 178, 107–115. https://doi.org/10.1016/0006-8993(79)90091-X

Johnson, J.-I., Fenske, B.A., Jaswa, A.S. & Morris, J.A. (2014) Exploitation of puddles for breakthroughs in claustrum research. *Frontiers in Systems Neuroscience*, 8, 78. https://doi.org/10.3389/fnsys.2014.00078

Karamanlidis, A.N., Saigal, R.P., Giolli, R.A., Mangana, O. & Michaloudi, H. (1979) Visual thalamocortical connections in sheep studied by means of the retrograde transport of Horseradish-Peroxidase. *Journal of Comparative Neurology*, 187(2), 245–259. https://doi.org/10.1002/cne.901870202

Kim, H.-G., Gu, Y.-N., Lee, K.-P., Lee, J.-G., Kim, C.-W., Lee, J.-W. *et al.* (2016) Immunocytochemical localization of the calcium-binding proteins calbindin D28K, calretinin, and parvalbumin in bat visual cortex. *Histology and Histopathology*, 31(3), 317–327 https://doi.org/10.14670/HH-11-680

Kowianski, P., Dziewiatkowski, J., Kowianska, J. & Morys, J. (1999) Comparative anatomy of the claustrum in selected species: a morphometric analysis. *Brain, Behavior and Evolution*, 53, 44–54.

Kowiański, P., Morys, J.M., Dziewiatkowski, J., Wojcik, S., Sidor-Kaczmarek, J. & Morys, J. (2008) NPY-, SOM- and VIP-containing interneurons in postnatal development of the rat claustrum. *Brain Research Bulletin*, 76, 565–571.

Krimmel, S.R., Qadir, H., Hesselgrave, N., White, M.G., Reser, D.H., Mathur, B.N. *et al.* (2019) Resting state functional connectivity of the rat claustrum. *Frontiers in Neuroanatomy*, 13, 22. https://doi.org/10.3389/fnana.2019.00022

Landzhov, B., Hinova-Palova, D., Edelstein, L., Dzhambazova, E., Brainova, I., Georgiev, G.P. *et al.* (2017) Comparative investigation of neuronal nitric oxide synthase immunoreactivity in rat and human claustrum. *Journal of Chemical Neuroanatomy*, 86, 1–14.

LeVay, S. & Sherk, H. (1981) The visual claustrum of the cat. I. Structure and connections. *The Journal of Neuroscience*, 1, 956–980. https://doi.org/10.1523/jneurosci.01-09-00956.1981

Lipowska, M., Kowianski, P., Majak, K., Jagalska-Majewska, H. & Morys, J. (2000) The connections of the endopiriform nucleus with the insular claustrum in the rat and rabbit. *Folia Morphol (Warsz)*, 59, 77–83.

Liu, J., Liu, B., Zhang, X.Y., Yu, B., Guan, W., Wang, K. *et al.* (2014) Development of the paralemniscal pathway in the barrel cortex. *Molecular Brain*, 7, 1–13. https://doi.org/10.1186/s13041-014-0084-8

Maçarico da Costa, N., Fürsinger, D. & Martin, K.A.C. (2010) The synaptic organization of the claustral projection to the cat's visual cortex. *Journal of Neuroscience*, 30, 13166–13170.

Mathur, B.N. (2014) The claustrum in review. *Frontiers in Systems Neuroscience*, 8, 1–11. https://doi.org/10.3389/fnsys.2014.00048

Mathur, B.N., Caprioli, R.M. & Deutch, A.Y. (2009) Proteomic analysis illuminates a novel structural definition of the claustrum and insula. *Cerebral Cortex*, 19, 2372–2379.

Melzer, S. Michael, M., Caputi, A., Eliava, M., Fuchs, E.c., Whittington, M.A. *et al.* (2012) Long-range-projecting GABAergic neurons modulate inhibition in hippocampus and entorhinal cortex. *Science*, 335, 1506–1510.

Meola, A., Comert, A., Yeh, F.C., Stefaneanu, L. & Fernandez-Miranda, J.C. (2015) The controversial existence of the human superior fronto-occipital fasciculus: connectome-based tractographic study with microdissection validation. *Human Brain Mapping*, 36, 4964–4971. https://doi.org/10.1002/hbm.22990

Minciacchi, D., Granato, A., Antonini, A., Tassinari, G., Santarelli, M., Zanolli, L. *et al.* (1995) Mapping subcortical extrarelay afferents on to primary somatosensory and visual areas in cats. *The Journal of Comparative Neurology*, 362, 46–70. 10.1002.cne.903620104

Narikiyo, K., Mizuguchi, R., Ajima, A., Shiozaki, M., Hamanaka, H., Johansen, J.P. *et al.* (2020) The claustrum coordinates cortical slow-wave activity. *Nature Neuroscience*, 23(6), 741–753. https://doi.org/10.1038/s41593-020-0625-7

Nitzsche, B., Frey, S., Collins, L.D., Seeger, J., Lobsien, D., Dreyer, A. *et al.* (2015) A stereotaxic, population-averaged T1w ovine brain atlas including cerebral morphology and tissue volumes. *Frontiers in Neuroanatomy*, 9, 1–14. https://doi.org/10.3389/fnana.2015.00069

Norita, M. (1977) Demonstration of bilateral claustro-cortical connections in the cat with the method of retrograde axonal transport of horseradish peroxidase. *Archivum Histologicum Japonicum*, 40(1), 1–10.

Olson, C.R. & Graybiel, A.M. (1980) Sensory maps in the claustrum of the cat. *Nature*, 288(5790), 479–481.

Orman, R., Kollmar, R. & Stewart, M. (2017) Claustrum of the short-tailed fruit bat, Carollia perspicillata: alignment of cellular orientation and functional connectivity. *The Journal of Comparative Neurology*, 525, 1459–1474.

Peruffo, A., Corain, L., Bombardi, C., Centelleghe, C., Grisan, E., Graïc, J.-M. *et al.* (2019) The motor cortex of the sheep: laminar organization, projections and diffusion tensor imaging of the intracranial pyramidal and extrapyramidal tracts. *Brain Structure and Function*, 224, 1933–1946. https://doi.org/10.1007/s00429-019-01885-x

Pirone, A., Castagna, M., Granato, A., Peruffo, A., Quilici, F., Cavicchioli, L. *et al.* (2014) Expression of calcium-binding proteins and selected neuropeptides in the human, chimpanzee, and crab-eating macaque claustrum. *Frontiers in Systems Neuroscience*, 8, 191–192. https://doi.org/10.3389/fnsys.2014.00099

Pirone, A., Magliaro, C., Giannessi, E. & Ahluwalia, A. (2015) Parvalbumin expression in the claustrum of the adult dog. An immunohistochemical and topographical study with comparative notes on the structure of the nucleus. *Journal of Chemical Neuroanatomy*, 64–65, 33–42.

Pirone, A., Cozzi, B., Edelstein, L., Peruffo, A., Lenzi, C., Quilici, F. *et al.* (2012) Topography of Gng2- and NetrinG2-expression suggests an insular origin of the human CL. *PLoS One*, 7(9), e44745.

Pirone, A., Miragliotta, V., Ciregia, F., Giannessi, E. & Cozzi, B. (2018) The catecholaminergic innervation of the claustrum of the pig. *Journal of Anatomy*, 232, 158–166. https://doi.org/10.1111/joa.12706

Pirone, A., Miragliotta, V., Cozzi, B. & Granato, A. (2019) The Claustrum of the pig: an immunohistochemical and a quantitative Golgi study. *Anatomical Record*, 302, 1638–1646. https://doi.org/10.1002/ar.24073

Pirone, A., Lazzarini, G., Lenzi, C., Giannessi, E. & Miragliotta, V. (2020) Immunolocalization of cannabinoid receptor 1 (CB1), monoglyceride lipase (MGL) and fatty-acid amide hydrolase 1 (FAAH) in the pig claustrum. *Journal of Chemical Neuroanatomy*, 109, 101843. https://doi.org/10.1016/j.jchemneu.2020.101843

Puelles, L., Ayad, A., Sandoval, J.E., Alonso, A., Medina, L. & Ferran, J.L. (2016a) Selective early expression of the orphan nuclear receptor Nr4a2 identifies the claustrum homolog in the avian mesopallium: impact on sauropsidian/mammalian pallium comparisons. *The Journal of Comparative Neurology*, 524, 665–703.

Rahman, F.E. & Baizer, J.S. (2007) Neurochemically defined cell types in the claustrum of the cat. *Brain Research*, 1159, 94–111.

Rausell, E., Bae, C.S., Viñuela, A., Huntley, G.W. & Jones, E.G. (1992) Calbindin and parvalbumin cells in monkey VPL thalamic nucleus: distribution, laminar cortical projections, and relations to spinothalamic terminations. *Journal of Neuroscience*, 12, 4088–4111.

Reynhout, K. & Baizer, J.S. (1999) Immunoreactivity for calciumbinding proteins in the claustrum of the monkey. *Anatomy and Embryology*, 199, 75–83.

Remedios, R., Logothetis, N.K. & Kayser, C. (2010) Unimodal responses prevail within the multisensory claustrum. *Journal of Neuroscience*, 30, 12902–12907. https://doi.org/10.1523/JNEUROSCI.2937-10.2010

Reser, D.H., Majka, P., Snell, S., Chan, J.M., Watkins, K., Worthy, K. *et al.* (2017) Topography of claustrum and insula projections to medial prefrontal and anterior cingulate cortex of the common marmoset (*Callithrix jacchus*). *The Journal of Comparative Neurology*, 525, 1421–1441.

Richard, P. (1967) *Atlas stéréotaxique du cerveau de Brebis "Préalpesdu-Sud"*. Paris: Institut National de la Recherche Agronomique.

Riche, D. & Lanoir, J. (1978) Some claustro-cortical connections in the cat and baboon as studied by retrograde horseradish persocidase transport. *Journal of Comparative Neurology*, 177(3), 435–444.

Rose, J.E. (1942) A cytoarchitectural study of the sheep cortex. *The Journal of Comparative Neurology*, 76(1), 1–55. https://doi.org/10.1002/cne.900760102

Sanides, D. & Buchholtz, C.S. (1979) Identification of the projection from the visual cortex to the claustrum by anterograde axonal transport in the cat. *Experimental Brain Research*, 34, 197–200.

Shang, C., Liu, Z., Chen, Z., Shi, Y., Wang, Q., Liu, S. *et al.* (2019) A parvalbumin-positive excitatory visual pathway to trigger fear responses in mice. *Science*, 348, 1472–1477.

Sherk, H. (1986). The claustrum and the cerebral cortex. In Jones, E.G. and Peters, A. (Eds.), *Sensory-motor areas and aspects of cortical connectivity. cerebral cortex*, vol. 5. Berlin: Springer, pp. 467–499. https://doi.org/10.1007/978-1-4613-2149-1_13

Squatrito, S., Battaglini, P.P., Galletti, C. & Riva, S.E. (1980) Projections from the visual cortex to the contralateral claustrum of the cat revealed by an anterograde axonal transport method. *Neuroscience Letters*, 19, 271–275.

Tanné-Gariépy, J., Boussaoud, D. & Rouiller, E.M. (2002) Projections of the claustrum to the primary motor, premotor, and prefrontal cortices in the macaque monkey. *Journal of Comparative Neurology*, 454(2), 140–157.

Tomioka, R. & Rockland, K.S. (2007) Long-distance corticocortical GABAergic neurons in the adult monkey white and gray matter. *The Journal of Comparative Neurology*, 505, 526–538.

Tremblay, R., Lee, S. & Rudy, B. (2016) GABAergic interneurons in the neocortex: from cellular properties to circuits. *Neuron*, 91(2), 260–292. https://doi.org/10.1016/j.neuron.2016.06.033

UniProt website. https://www.uniprot.org/uniprot/?query=calbindin+sheep&sort=score), accessed on 07/04/2020

Vanderwolf, C.H. & Cooley, R.C. (2002) *The sheep brain: a photographic series*, 2nd ed. London: A J Kirby & Co.

Vertes, R.P. & Hoover, W.B. (2008) Projections of the paraventricular and paratenial nuclei of the dorsal midline thalamus in the rat. *The Journal of Comparative Neurology*, 508, 212–237.

Walk, R.D. & Gibson, E.J. (1961) A comparative and analytical study of visual depth perception. *Psychological Monographs: General and Applied*, 75, 1–44.

Wang, Q., Ng, L., Harris, J.A., Feng, D., Li, Y., Royall, J.J. *et al.* (2017) Organization of the connections between claustrum and cortex in the mouse. *The Journal of Comparative Neurology*, 1346, 1317–1346.

Watakabe, A. (2017) In situ hybridization analyses of claustrumenriched genes in marmosets. *The Journal of Comparative Neurology*, 525, 1442–1458.

Watson, C. & Puelles, L. (2017) Developmental gene expression in the mouse clarifies the organization of the claustrum and related endopiriform nuclei. *Journal of Comparative Neurology*, 525(6), 1499–1508. https://doi.org/10.1002/cne.24034

White, M.G. & Mathur, B.N. (2018) Frontal cortical control of posterior sensory and association cortices through the claustrum. *Brain Structure and Function*, 223, 1–8. https://doi.org/10.1007/s00429-018-1661-x

Yeh, F.C., Verstynen, T.D., Wang, Y., Fernández-Miranda, J.C. & Tseng, W.Y.I. (2013) Deterministic diffusion fiber tracking improved by quantitative anisotropy. *PLoS One*, 8(11), e80713.

Yu, S.-H., Lee, J.-Y. & Jeon, C.-J. (2011) Immunocytochemical localization of calcium-binding proteins, calbindin D28K-, calretinin-, and parvalbumin-containing neurons in the dog visual cortex. *Zoological Science*, 28(9), 694–702. https://doi.org/10.2108/zsj.28.694

SUPPORTING INFORMATION

Additional supporting information may be found online in the Supporting Information section.

How to cite this article: Pirone A, Graïc JM, Grisan E, Bruno C. The claustrum of the sheep and its connections to the visual cortex. *J. Anat*. 2021;238:1–12. https://doi.org/10.1111/joa.13302